CrystEngComm

Architecting layered molecular packing in substituted benzobisbenzothiophene (BBBT) semiconductor crystals

Journal:	*CrystEngComm*
Manuscript ID	CE-ART-02-2020-000285.R1
Article Type:	Paper
Date Submitted by the Author:	17-Apr-2020
Complete List of Authors:	Higashino, Toshiki; National Institute of Advanced Industrial Science and Technology (AIST) Arai, Shunto; The University of Tokyo Inoue, Satoru; The University of Tokyo Tsuzuki, Seiji; National Institute of Advanced Industrial Science and Technology (AIST) Shimoi, Yukihiro; National Institute of Advanced Industrial Science and Technology (AIST) Horiuchi, Sachio; National Institute of Advanced Industrial Science and Technology (AIST) Hasegawa, Tatsuo; The University of Tokyo Azumi, Reiko; National Institute of Advanced Industrial Science and Technology (AIST)

ARTICLE

Architecting layered molecular packing in substituted benzobisbenzothiophene (BBBT) semiconductor crystals

Received 00th January 20xx,
Accepted 00th January 20xx

DOI: 10.1039/x0xx00000x

Toshiki Higashino,*[a] Shunto Arai,[b] Satoru Inoue,[b] Seiji Tsuzuki,[c] Yukihiro Shimoi,[c] Sachio Horiuchi,[a] Tatsuo Hasegawa*[b] and Reiko Azumi[a]

Construction and control of 2D layered packing motifs with π-extended fused-ring molecules is of crucial importance for developing organic electronic materials and devices. Herein, we demonstrate that, when adequately substituted, two kinds of layered packing motifs are obtainable for benzo[1,2-b:4,5-b']bis[b]benzothiophene (**BBBT**), which itself does not show layered crystallinity. We synthesized BBBT derivatives substituted with a combination of alkyl chains and a phenyl ring in a symmetric/unsymmetric manner; 2,8-didecyl-BBBT (**diC10-BBBT**) and 2-decyl-8-phenyl-BBBT (**Ph-BBBT-C10**). We found that **diC10-BBBT** forms a layered π-stack (LπS) structure mainly composed of slipped parallel stacks, while **Ph-BBBT-C10** forms a typical layered herringbone (LHB) packing chiefly composed of T-shaped contacts. The feature is associated with the non-layered packing motif in **BBBT**: typical π-stack and herringbone structures, both of whose polymorphs show a large slip along the molecular long axis. Calculations of intermolecular interaction energies between neighbouring molecules in the crystals reveal that the interchain interactions suppress the long-axis slip, leading to the formation of the LπS and the LHB, respectively. Both **diC10-BBBT** and **Ph-BBBT-C10** form uniform (ultra)thin films originating from the layered crystallinity, and exhibit good transistor characteristics with hole mobility of about 1 $cm^2 V^{-1} s^{-1}$. We discuss how the substituent modifications are useful as crystal engineering to explore the potential of π-extended molecules for electronic applications.

Introduction

π-Extended fused-ring compounds based on (thieno)acenes are attracting considerable attentions as they constitute the fundamental material base for organic electronic applications.[1-10] The compounds feature extended π-electronic states over the backbones as well as relatively strong intermolecular π-π interactions, allowing efficient charge transport. A significant and essential requirement for their use in organic thin-film transistors (TFTs) is to achieve high layered crystallinity, because the self-organizing architecture of a 2D molecular packing geometry is most suitable for obtaining perfectly aligned semiconductor-insulator interfaces.[11,12] In fact, high-performance organic TFTs have been reported in pentacene,[13-16] rubrene,[17-20] benzothieno[3,2-b][1]benzothiopene (BTBT),[21-25] dinaphtho[2,3-b:2',3'-f]thieno[3,2-b]thiophene (DNTT),[26-29] and others[30-39] that involve layered packing motifs.

However, it is also known that the layered packing geometry is not usually seen in the π-extended fused-ring compounds without substitution modification. The crystal structures of the compounds are traditionally categorized into herringbone, π-stack (γ type), and several others, in terms of the shortest cell length and the interplanar angle between adjacent molecules.[40,41] The molecular layer formation due to the side-by-side intermolecular contacts is not seen in many compounds,[42-45] because pairs of some neighbouring molecules are only partially overlapped with each other along the molecular long axes, (or the molecules exhibit long-axis slip to each other) within the crystals. The feature should be ascribed to the relatively unfavourable nature of the intermolecular face-to-edge (T-shaped) or face-to-face (parallel π-stack) contacts over the whole length of the molecules.[46,47] It means that most

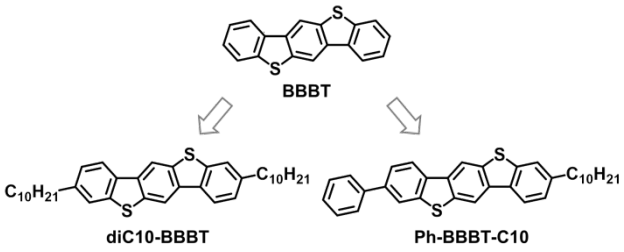

Chart 1 Molecular structures of **diC10-BBBT** and **Ph-BBBT-C10**.

[a] *Electronics and Photonics Research Institute, National Institute of Advanced Industrial Science and Technology (AIST), Tsukuba, 305-8565, Japan. E-mail: t-higashino@aist.go.jp*
[b] *Department of Applied Physics, The University of Tokyo, Tokyo, 113-8656, Japan. E-mail: t-hasegawa@ap.t.u-tokyo.ac.jp*
[c] *Research Center for Computational Design of Advanced Functional Materials (CD-FMat), National Institute of Advanced Industrial Science and Technology (AIST), Tsukuba, 305-8568, Japan.*

† Additional information for Synthetic procedures and characterization data, thermal gravimetric analysis (TGA), differential scanning calorimetry (DSC), single crystal determination, Hirshfeld surface analysis, intermolecular interaction energy calculation, thin-film characterization, and TFT characteristics. CCDC 1964819 and 1964820 contain the supplementary crystallographic information for compound **diC10-BBBT** and **Ph-BBBT-C10**, respectively. For ESI and crystallographic data in CIF or other electronic format see DOI: 10.1039/x0xx00000x

of the π-extended fused-ring compounds are not suitable for fabricating organic TFTs as their parent molecules. Thus, "crystal engineering" would be indispensable for exploring the further potential of the π-extended fused-ring compounds.

Various substitution effects on the π-extended fused-ring compounds have been studied, so far, for their use in organic TFTs. For example, several reports show that silylethynyl substitutions at the peri-position of (hetero)acenes are useful to enhance the π-stack-type molecular packing.[48-50] The effect of other substituents, such as methyl,[51,52] butyl,[53-56] methoxy,[57-59] or halogen[60-62] groups was also investigated. It was also suggested that long-alkyl-chain substitutions on π-conjugated molecules work as "molecular fastener" (or zipper) effect to enhance the intermolecular π-π interactions.[27,63-66] Nonetheless, the methodology of crystal engineering has not yet been established.

Recently, it was demonstrated that relatively long alkyl-chain substitution on the BTBT or benzothieno[3,2-b]naphtho[2,3-b]thiophene (BTNT) backbones is effective and useful for enhancing the layered crystallinity, on the basis of systematic investigation on the effect of substituted chain length on the compounds[67-70]: 1) The long alkyl-chain substitution allows the formation of aligned alkyl-chain layers, which is effective for achieving the layered-herringbone (LHB) packing, while the relatively short alkyl-chain substitution destroys the layered packing motif;[67,68] 2) Unsymmetrical substitution with an alkyl chain seems to be more favourable for enhancing the layered crystallinity compared to symmetrical substitution with a pair of alkyl chains, as the former forms bilayer-type molecular packing motifs;[71-76] 3) The phenyl ring substitution also contributes to enhancing the layered crystallinity by the herringbone-type arrangement of benzene rings;[70,77] and 4) The crystalline stability is enhanced due to the alkyl-chain layer formation, as is confirmed by high-precision quantum chemical calculations for the intermolecular interaction energies.[68,78] Despite these findings, however, the effect of the substitutions on other kinds of π-extended fused-ring backbones is unknown as the studies are limited to the BTBT derivatives that originally involves the layered packing motif when unsubstituted.

Here, we focus on an extended linear thienoacene compound, benzo[1,2-*b*:4,5-*b'*]bis[*b*]benzothiophene (**BBBT**, Chart 1). The BBBT skeleton is categorized as a five-ring-fused thienoacene family, in which a benzene ring is fused in the middle of the BTBT skeleton. The BBBT skeleton forms a non-layered structure due to a large molecular slip along the long-axis direction and forms two types of polymorphs: a typical π-stack and a herringbone packing motif.[79,80] As the large long-axis slip eliminates the layered crystallinity, the thin films of **BBBT** and its derivatives reported so far did not show sufficiently good organic TFT characteristics (mobilities of ~10^{-2} cm^2 V^{-1} S^{-1}). We developed two kinds of substituted BBBTs tailored by introducing a combination of long alkyl chains and a phenyl ring in a symmetrical/unsymmetrical manner: 2,8-didecyl-BBBT (**diC10-BBBT**, chart 1) and 2-decyl-8-phenyl-BBBT (**Ph-BBBT-C10**), and successfully achieved two different kinds of layered packing motifs: layered π-stack (LπS) and layered herringbone (LHB) packing motifs, respectively. We investigated the origin of the structural change based on calculations of intermolecular interaction energies, and the thin-film and TFT characteristics of **diC10-BBBT** and **Ph-BBBT-C10**. Based on the results, we discuss how these substituent modifications are a useful crystal engineering method for achieving high layered crystallinity and thereby exploring the potential of these compounds for organic electronic applications.

Results and discussion

Basic molecular characteristics. In the synthesis of **Ph-BBBT-C10**, an unsymmetric precursor was first synthesized in the presence of two kinds of coupling partners with a decyl chain and a phenyl group. Then, the BBBT backbones were formed via double intramolecular cyclization using two methylsulfinyl groups within the precursor, as outlined in Scheme S1.[80] The materials were sufficiently soluble in chlorinated or aromatic solvents. The solvent solubilities in chlorobenzene, *o*-xylene, and chloroform at 25 °C were 71, 49, and 61 mmol/L for **diC10-BBBT** and 1.9, 1.1, and 1.4 mmol/L for **Ph-BBBT-C10**, respectively.

The TG-DTA and DSC curves for **diC10-BBBT** and **Ph-BBBT-C10** are shown in Figure S1. Three endothermic peaks are observed in both **diC10-BBBT** and **Ph-BBBT-C10**. The peaks observed at the highest temperatures correspond to the melting points; 208 °C for **diC10-BBBT** and 347 °C for **Ph-BBBT-C10**. The other peaks are due to liquid-crystal (LC) transitions, as is similar to other alkylated thienoacenes.[67,68,71,72] The transition temperature from the crystal phase to the LC phase is much higher in **Ph-BBBT-C10** (at 211 °C) than in **diC10-BBBT** (at 98 °C).

The comparison of the solvent solubility and the crystal-phase stability are clearly associated with each other in these compounds; **Ph-BBBT-C10** is much less soluble and more

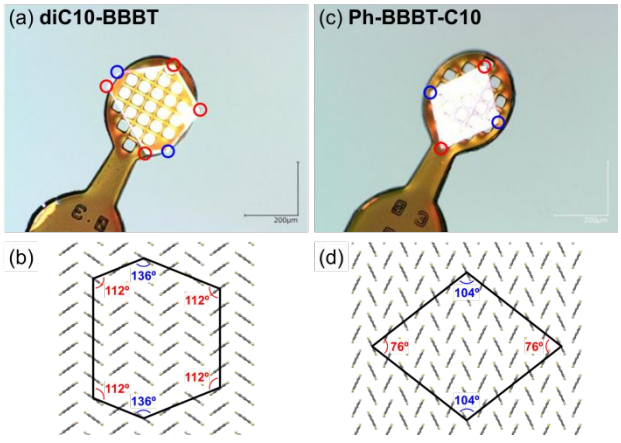

Fig. 1 Crystal shapes and molecular arrangements of (a)(b) **diC10-BBBT** and (c)(d) **Ph-BBBT-C10**. (a)(c) Crossed-Nicols polarized micrographs of single crystals obtained by recrystallization from anisole/ethanol mixed solution and fixed on mesh-type LithoLoops. (b)(d) Molecular arrangements in the two-dimensional layer and schematic crystal shapes (black line) within the interior angles, that corresponds to coloured circles in panels a and c (C10 chains and phenyl groups are omitted for clarity).

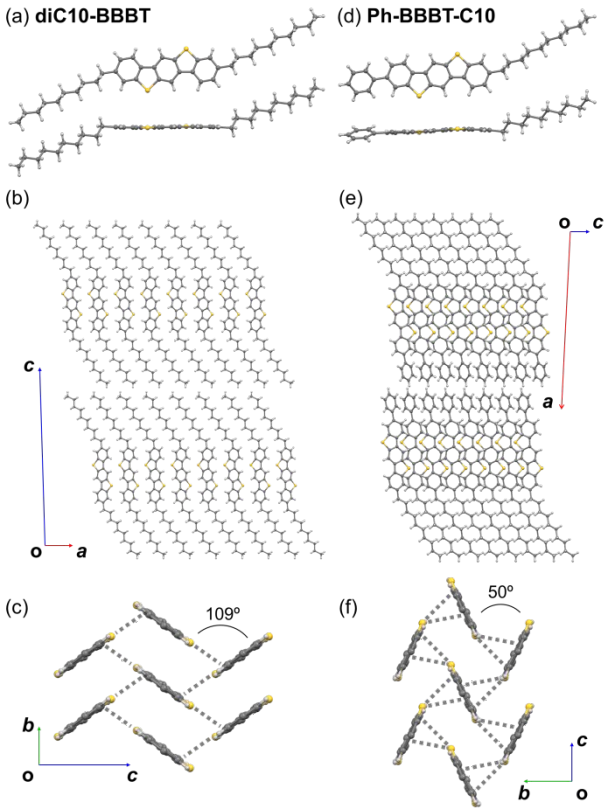

Fig. 2 Crystal structures of (a-c) **diC10-BBBT** and (d-f) **Ph-BBBT-C10**. (a)(d) Top and front views of one molecule. (b)(e) Projection along the crystal *b* (molecular stacking) axis. (c)(f) Projection along the crystal *a* (molecular long) axis (C10 chains and Ph groups are omitted for clarity; gray broken lines show S···C short contacts: 3.57897(9) and 3.58520(9) Å for **diC10-BBBT**, 3.373(3), 3.394(3), 3.428(3), 3.434(3), 3.472(3) and 3.486(3) Å for **Ph-BBBT-C10**.

thermally stable than **diC10-BBBT**. This is because an alkyl chain should increase the entropy of dissolution more than a phenyl group, originating from the appearance of various conformers associated with the *trans* and *gauche* conformations of the alkyl chain in liquid phase.[81] We note that the comparison between **Ph-BBBT-C10** and **Ph-BTBT-C10**[67,71] is basically understood in terms of the π-extension effect; the latter presents the higher solubility (~ 5 mmol/L for chlorobenzene) and lower crystal-LC transition temperature (143 °C) than the former, as shown in Figure S2. In contrast, the comparison between **diC10-BBBT** and **diC10-BTBT**[22,68] is not straightforward; the latter presents lower solubility (~ 50 mmol/L for chloroform) and higher crystal-LC transition temperature (112 °C) than the former. These results imply that the crystal lattice energies of **Ph-BBBT-C10** and **diC10-BBBT** are quite distinct, taking into account the fact that both **Ph-BTBT-C10** and **diC10-BTBT** have almost the same herringbone-type molecular packing in crystal.[67,68]

Crystal packing motifs. The **diC10-BBBT** single crystal tends to grow as a hexagonal plate (Figure 1a), while the **Ph-BBBT-C10** crystal is a rhomboid plate (Figure 1c), both with excellent crystal quality. The crystallographic data are listed in Table S1. We successfully executed reliable crystal structure analyses as shown in the Table S1. The **diC10-BBBT** belongs to the monoclinic system, space group *C*2/*c* (#15), while **Ph-BBBT-C10** belongs to $P2_1/c$ (#14). In the **diC10-BBBT** crystal, the BBBT skeletons are almost planar, and the decyl chains stretch out, having a typical antiperiplanar conformation without any disorder, as shown in Figure 2a. In contrast in the **Ph-BBBT-C10**, the BBBT core and the phenyl group are twisted with a torsion angle of about 24°, as shown in Figure 2d.

The molecules form the characteristic layered structures without any molecular long-axis slip in both **diC10-BBBT** and **Ph-BBBT-C10**, as presented in Figures 2b and 2e. The layered structures are classified according to the symmetrical/unsymmetrical substitution: **diC10-BBBT** shows a typical lamellar-type structure, whereas **Ph-BBBT-C10** exhibits a bilayer-type structure involving a head-to-head-type contact.

The molecular short-axis orientations within the 2D layer of these compounds are also distinct with each other, as depicted in Figures 2c and 2f. The dihedral angles formed by two alternating BBBT planes are considerably different, about double: 109° for **diC10-BBBT** and 50° for **Ph-BBBT-C10**. According to the relationship between the dihedral angles and the shortest cell axes (4.29828(11) Å for **diC10-BBBT** and 6.13566(16) Å for **Ph-BBBT-C10**), the BBBT arrangements are classified into a π-stack packing for **diC10-BBBT** and a herringbone packing for **Ph-BBBT-C10**.[41,42] This classification is also supported by the Hirshfeld surface analysis and fingerprint plots.[82] As shown in Figures S3 and S4, the (C···H)/(C···C) ratio is estimated to be 3.4/1 for **diC10-BBBT** and 41/1 for **Ph-BBBT-C10**, respectively. The result indicates that the face-to-face (π-stack) contact dominates over the edge-to-edge (we call "*L*-shape") contact in the former, whereas the face-to-edge (*T*-shape) contact dominates the latter. Note that the ratio under or over 5/1 is a criterion to classify between the π-stack packing and a herringbone packing, according to the literature.[82]

We here comment that the appearance of the crystal shape, shown in Figures 1b and 1d, is closely associated with the molecular packing motifs in the compounds. For **Ph-BBBT-C10**, all four sides of the rhomboid are originated in the direction along the *T*-shaped contacts. In contrast, for **diC10-BBBT**, four sides of the hexagon correspond to the *L*-shaped contacts and the other two are due to the π-stack direction.

Substitution effect on packing motifs. Figures 3a and 3b summarize the molecular arrangements in **diC10-BBBT** and **Ph-BBBT-C10**, with those of the reported BBBT derivatives. As reported by Takimiya and Müllen, **BBBT** crystallizes into the two types of polymorphs; phase A and B.[79,80] The dihedral angle of the BBBT plane is 57° in phase A, which is assigned as a herringbone packing, whereas that is 125° in phase B, which is assigned as a π-stack. A major feature common to both polymorphs is the non-layered structure with a large molecular slip along the long-axis direction between adjacent molecules. This feature remains after the dibutyl (diC4-)substitution on the BBBT core: the substitution results in the long-axis slip, although the resultant interlayer contact is only formed between the alkyl chains.[80] Instead, the BBBT cores form purely 1D π-stack

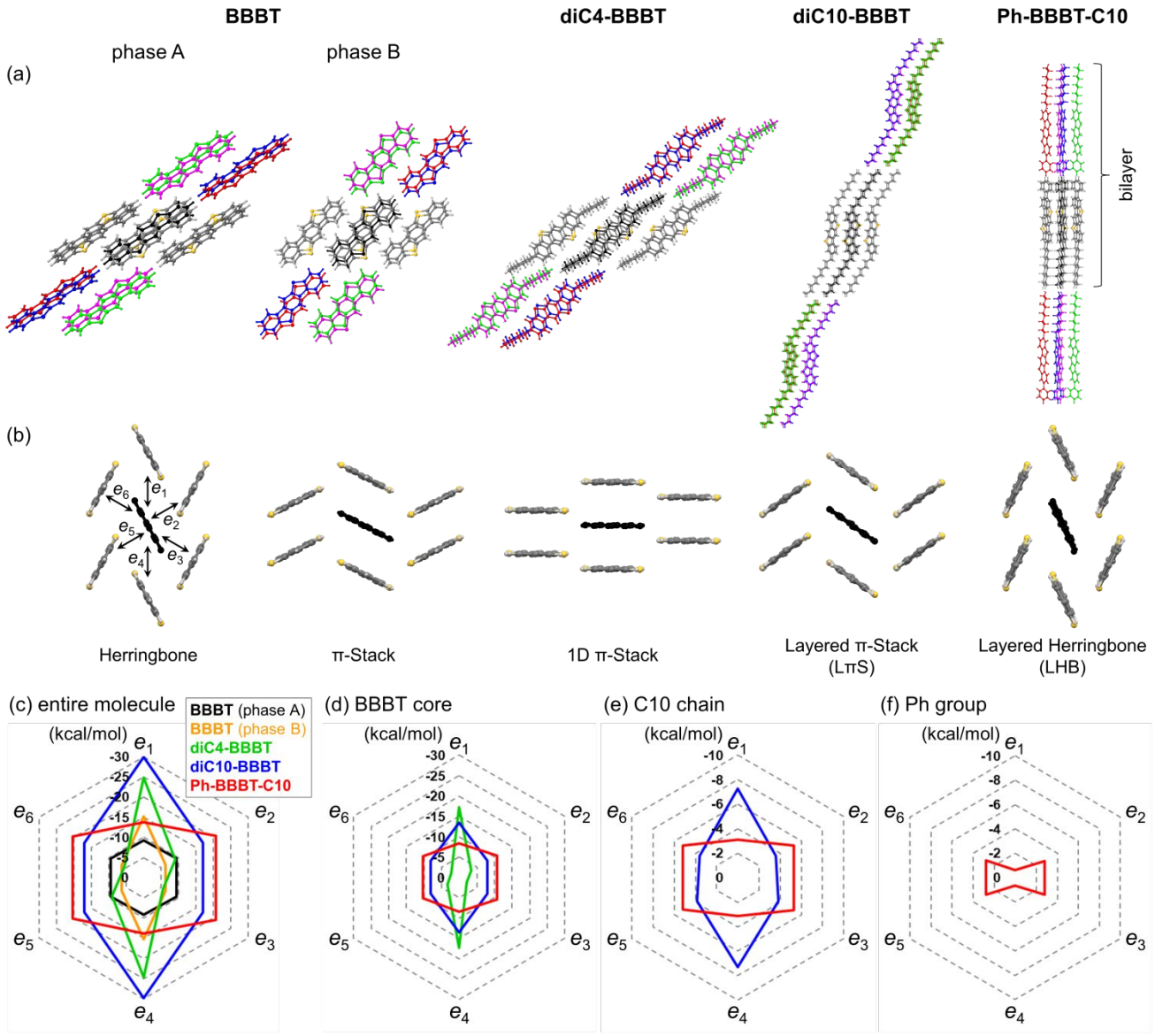

Fig. 3 Molecular arrangements and intermolecular interaction energies of **BBBT** (polymorphic crystal phases A and B),[79,80] **diC4-BBBT**,[80] **diC10-BBBT**, and **Ph-BBBT-C10**. Molecular arrangements (a) viewed along the molecular stacking direction of the central black-coloured molecule and the surrounding molecules, and (b) viewed along the molecular long axis of the central molecule and the six nearest intralayer counterparts (C10 chains and Ph groups are omitted for clarity). Intermolecular interaction energies along the *translational* (e_1 and e_4) and the *diagonal* (e_2, e_3, e_5, and e_6) directions depicted in panel b, calculated by using the empirical atomic coordinates of (c) the entire molecule, (d) the extracted BBBT core, (e) the extracted C10 chain, and (f) the extracted Ph group.

without short-axis slip or the roll in the short-axis orientations of the BBBT backbones. The conventional herringbone or 'rolled' π-stack structure,[83] as seen in **BBBT**, are lost.

By contrast, **diC10-BBBT** and **Ph-BBBT-C10** clearly present the layered structures, as described above. It means that the molecules are 'forced' to form layered structures by the symmetric/unsymmetric introduction of a combination of long alkyl chains and a phenyl ring, even for the BBBT backbone that inherently forms non-layered structures. Meanwhile, in terms of the backbone arrangements, the herringbone and the 'rolled' π-stack structures, as seen in **BBBT**, are restored in **Ph-BBBT-C10** and **diC10-BBBT**, respectively. The effect of architecting layered molecular packing is apparent with the long-alkyl-chain substitutions.

Classification by intermolecular interactions. Calculated intermolecular interaction energies are summarized in Figure 3c; those between the central black-coloured molecule (in Figures 3a and 3b) and the six nearest short-axis counterparts in the *translational* (e_1 and e_4) and *diagonal* (e_2, e_3, e_5, and e_6) directions for all the compounds. All the results of the calculations are presented in Figures S5–S9. Following interesting features are seen in the plot: Interaction distribution is close to a regular hexagon in the herringbone packing of

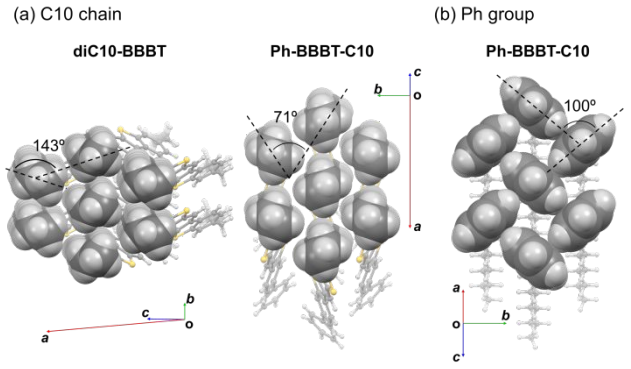

Fig. 4 Molecular arrangements focusing on (a) the C10 chains and (b) the phenyl group in **diC10-BBBT** and **Ph-BBBT-C10**.

'phase A' of **BBBT**. In contrast, the size ratio between the *diagonal* and *translational* contacts is around 3:2 in the LHB of **Ph-BBBT-C10**, as is consistent with those in the LHB of other materials.[67,68] We also found that the ratio around 3:2 holds, in consideration of the 'interlayer' contact by the long-axis slip, in the 'phase A' of **BBBT** (see Figure S5). In contrast, in the π-stack structures (*i.e.*, 'phase B' of **BBBT**, **diC4-BBBT**, and **diC10-BBBT**), the interaction energies at the *translational* contacts are roughly two times larger than that at the *diagonal* contacts, or the plots is like an elongated hexagon.

To gain further insight into the origin of the structure formation, we investigated the contribution of respective parts of molecules to the intermolecular interaction energies, the results of which are shown in Figures 3d-3f. It is interesting to find out that the shape of the plot for the interaction energies between BBBT backbones (Figure 3d) are roughly identical to that for the interaction energies between entire molecules in any of **diC4-BBBT**, **diC10-BBBT**, and **Ph-BBBT-C10**. The shape of the plot for the interaction energies between the decyl chains in **diC10-BBBT** and **Ph-BBBT-C10** are also nearly identical to that for entire molecules (Figure 3e), respectively, which is ascribed to the different dihedral angles between the all-*trans* zigzag chain planes (143° for **diC10-BBBT** and 71° for **Ph-BBBT-C10**, Figure 4a), indicating that the decyl-chain arrangements in **diC10-BBBT** and **Ph-BBBT-C10** should also be classified as a π-stack and a herringbone fashion, respectively. The phenyl group in **Ph-BBBT-C10** forms nearly orthogonal arrangement in a herringbone-type manner (Figure 4b), and shows quasi-2D interaction energies along the *diagonal* directions (Figure 3f). These features should be the key to achieve the LHB packing motif in **Ph-BBBT-C10**.

Intermolecular transfer integrals. Figure 5 shows calculated intermolecular transfer integrals for **diC10-BBBT** and **Ph-BBBT-C10**. As expected, relatively high anisotropy (or 1D nature) along the π-stack is seen in the intermolecular transfer integrals for **diC10-BBBT**, where both HOMO and HOMO-1 should contribute almost equally to the carrier transport. In contrast, roughly isotropic (or 2D) nature is seen in the intermolecular transfer integrals within the layer of **Ph-BBBT-C10**. Additionally, the contribution of HOMO-1 to the carrier transport should be much smaller than that of HOMO in **Ph-BBBT-C10**. The feature should be ascribed to the fact that the HOMO−1 in **Ph-BBBT-C10** has nodes on the sulphur atoms, which diminishes the orbital overlap between neighbouring molecules.[84-86]

Film forming ability. Figure S10 summarizes the usual optical micrographs, the crossed-Nicols polarized micrographs, and the AFM height images of the blade-coated films for **diC10-BBBT** and **Ph-BBBT-C10**. Crystalline thin films with multiple domains are obtained for the both. Among them, **diC10-BBBT** forms relatively thick films with thickness of about tens of nanometre. A step height of about 3.5 nm that corresponds to the single-layer thickness is observed in the films. In contrast, **Ph-BBBT-C10** forms highly uniform ultrathin films composed of only a single bilayer thickness of about 5.6 nm. By optimizing the film-forming conditions, it is possible to obtain a large-area single-domain and single-bilayer film in **Ph-BBBT-C10**, as shown in Figure S11. The results demonstrate that the layered crystallinity is effectively enhanced by the formation of bilayer-type LHB packing motif.

TFT characteristics. Typical *p*-type characteristics are observed for the TFTs of both **diC10-BBBT** and **Ph-BBBT-C10**, as seen in Figure 6 and S12. The saturation mobilities are estimated as high as 1 $cm^2 V^{-1} s^{-1}$ for **diC10-BBBT** and 0.3 $cm^2 V^{-1} s^{-1}$ for **Ph-BBBT-C10**, respectively. These values are two orders of magnitude higher than those of **BBBT** and **diC4-BBBT**.[79,80] These results clearly demonstrate that the 2D layered

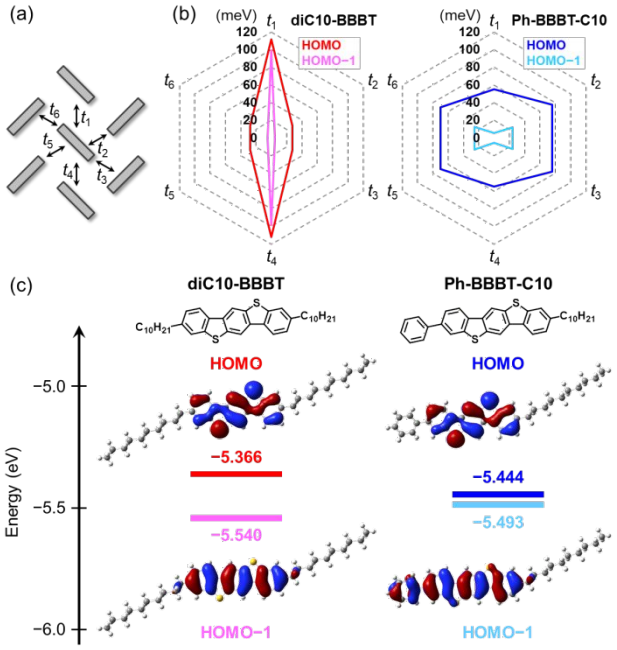

Fig. 5 Schematic herringbone-like packing motif and (b) the corresponding transfer integrals calculated by ADF program package at PW91/TZP level using HOMO and HOMO−1, respectively, and (c) HOMO and HOMO−1 energy levels and distribution maps of **diC10-BBBT** and **Ph-BBBT-10**.

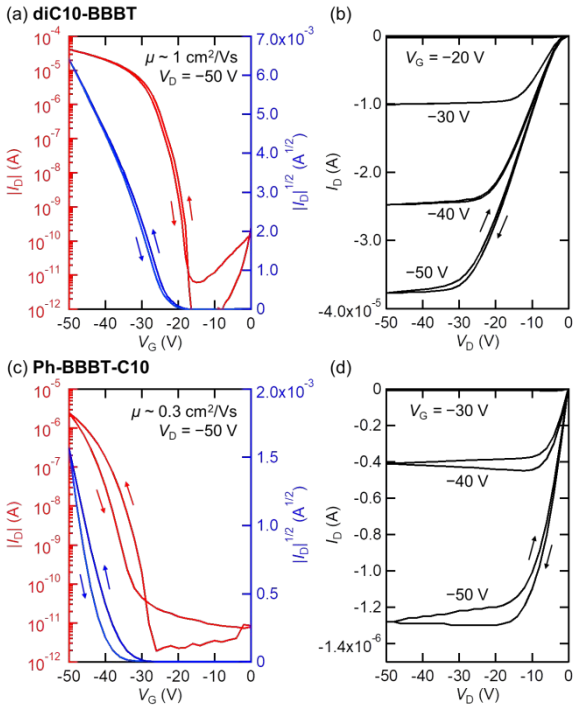

Fig. 6 (a)(c) Transfer and (b)(d) output characteristics of the solution-crystallized TFT devices: (a)(b) **diC10-BBBT** and (c)(d) **Ph-BBBT-10**.

structure is suitable to afford channel layers of organic TFTs allowing efficient charge carrier transport. In both the transfer and output characteristics, the hysteresis is negligibly small for the **diC10-BBBT** TFTs, in contrast to the large observed hysteresis for the **Ph-BBBT-C10** TFTs. This is probably due to the backgate effect on the channel layer, which becomes more sensitive in case of thinner semiconducting layers.[87-79] In the output characteristics, the thick **diC10-BBBT** film shows a fairly nonlinear feature in the low-voltage region, whereas the ultrathin film of **Ph-BBBT-C10** shows a nearly ohmic behaviour. This nonlinearity could be ascribed to the difference in the thickness: the thicker film tends to give larger access resistance between the channel and the source-drain electrodes, owing to the existence of alkyl chain layers within the crystals.[90]

Conclusions

We have successfully synthesized two kinds of layered-crystalline organic semiconductor compounds, **diC10-BBBT** and **Ph-BBBT-C10**, in which a combination of decyl chains and a phenyl group is utilized to substitute, in a symmetric/unsymmetric manner, whereas the unsubstituted parent BBBT backbone does not show layered-crystallinity. The symmetrically-substituted **diC10-BBBT** forms the LπS structure mainly featured by the intralayer π-stacks of the BBBT cores. The unsymmetrically-substituted **Ph-BBBT-C10** forms the bilayer-type LHB motif which is featured by the intralayer *T*-shaped and slipped-parallel contacts. Appearance of these layered packing motifs is closely associated with the two types of polymorphs of **BBBT**, exhibiting conventional π-stack and herringbone structures although the both involve large long-axis slip between adjacent molecules. DFT calculations for the intermolecular interaction energies revealed that the classification between the LπS and LHB packings are clearly associated with the non-layered π-stack and herringbone packings, respectively. The calculations also revealed that the long-alkyl-chain substitution and phenyl substitution take crucial roles in achieving the layered molecular packings. Both **diC10-BBBT** and **Ph-BBBT-C10** show high film-forming ability, and particularly **Ph-BBBT-C10** allows to form highly uniform ultrathin films, due to the high layered crystallinity which is characteristic of the bilayer-type LHB packing. Both **diC10-BBBT** and **Ph-BBBT-C10** exhibit good transistor characteristics with hole mobilities of ~1 cm^2 V^{-1} s^{-1}. The findings clearly demonstrate the effect of substituent modifications on architecting 2D layered molecular packing for BBBT skeleton, although the methodology itself as crystal engineering might be in a premature stage, when considering a vast variety of π-extended fused-ring compounds and substitutions. We believe that these findings are important for designing and developing a new class of layered-crystalline materials for ultrathin printed/flexible electronics.

Experimental

Materials synthesis. The procedure for synthesizing the title compounds, **diC10-BBBT** and **Ph-BBBT-C10**, is summarized in the Supporting Information.

Thermal properties. Thermal properties were investigated by thermogravimetry–differential thermal analysis (TG-DTA; STA7200RV, Hitachi High-Tech Science Co.) and differential scanning calorimetry (DSC; DSC7000X, Hitachi High-Tech Science Co.). TG-DTA measurements were performed in a range between room temperature and 500 °C at a heating rate of 5 K/min under N_2. For the DSC measurements, the sample was heated and subsequently cooled at a rate of 10 K/min for the first cycle and 5 K/min for the second cycle under N_2. The obtained TG-DTA and DSC curves are shown in Figure S1.

Crystal growth. Single crystals of **diC10-BBBT** and **Ph-BBBT-C10** were obtained by recrystallization from the concentrated solutions. Recrystallization from an anisole/ethanol mixed solution affords plate (flake)-like thin crystals as presented in Figures 1a and 1c.

X-ray diffraction and structure analysis. The single-crystal X-ray diffraction data were collected by using a Rigaku AFC10 four-circle diffractometer equipped with a Pilatus 200 K hybrid pixel detector and a graphite monochromated MoKα radiation source (λ = 0.71073 Å) for **diC10-BBBT**, and a Rigaku VariMax Dual four-circle diffractometer with a monochromated CuKα radiation source (λ = 1.5418 Å) for **Ph-BBBT-C10**. Data reduction with empirical absorption correction was performed using the CrysAlisPro software package.[91] The structure was solved by the direct method using the SIR2004 program[92] and was refined by

the full-matrix least squares method using SHELXL[93] by applying anisotropic temperature factors for all non-hydrogen atoms. All the hydrogen atoms were also determined from the experimental data. The crystallographic data are listed in Table S1.

Hirshfeld surface analysis. Hirshfeld surface analysis was utilized to classify the intermolecular van der Waals contacts. The Hirshfeld surfaces[94,95] and the associated fingerprint plots[96] were calculated with use of *CrystalExplorer*[97] for **BBBT** (phase A and phase B), **diC4-BBBT**, **diC10-BBBT**, and **Ph-BBBT-C10**. The results are summarized in Figures S3 and S4.

Density functional theory calculation. Density functional theory (DFT) calculations for the intermolecular interaction energies between neighboring molecules were performed using the Gaussian16 program package,[98] based on the experimental crystal geometries. The intermolecular interaction energies were calculated at the B3LYP/6-311G** level with Grimme's D3 dispersion correction.[99] The basis set superposition error (BSSE)[100] was corrected by the counterpoise method.[101] The interaction energies between the BBBT cores, between the C10 chains, and between the Ph groups were calculated, respectively, using the fragment structures in the crystals. The dangling bonds of the fragments were capped by hydrogen atoms in the calculations.

The transfer integrals between neighboring molecules were calculated by the Amsterdam Density Functional (ADF) program package[102] at the PW91/TZP level using the respective HOMO and HOMO−1 generated from the empirical atomic coordinates.

Thin-film processing. A 0.1 wt% chlorobenzene (Sigma-Aldrich, 99.9%) solution of **diC10-BBBT** and a 0.05 wt% solution of **Ph-BBBT-C10** were used for thin-film fabrication employing a blade-coating technique. A heavily *p*-doped Si wafer covered with a 100 nm thermally grown SiO_2 dielectric layer was used as a substrate after being cleaned by sequential sonication in deionized water, acetone, 2-propyl alcohol, and deionized water. A thin glass plate coated with Cytop (CTL-809M; AGC Inc., Japan) was used as the coating blade, and its motion was controlled by a stepping motor (SHOT-302GS; Sigmakoki Co., Ltd., Japan). Blade-coating was performed at a sweep rate ranging from 0.5 to 2.5 μm/s, under ambient conditions.

Atomic force microscopy (AFM) images of the single-crystalline thin films of **diC10-BBBT** and **Ph-BBBT-C10** were recorded on a Dimension 3000/Nanoscope IIIa system (Bruker Co., Ltd., USA) in the tapping mode under ambient conditions.

Fabrication of TFTs. Source/drain electrodes were patterned on the blade-coated thin films of **diC10-BBBT** and **Ph-BBBT-C10** by thermal deposition of gold using a shadow mask; the channel length and width were 200 and 500 μm, respectively. For proper mobility evaluation, parts of the thin films outside the channel were trimmed away using a micromanipulator (Axis-Pro; Systems Engineering Inc., Japan). Two-probe characteristics of bottom-gate top-contact TFTs were measured under N_2 by using a Precision Source/Measure Unit (B2912A; Keysight Technologies, USA).

Conflicts of interest

There are no conflicts to declare.

Acknowledgements

This study was partly supported by JSPS KAKENHI Grant Numbers 18H03875 and 18K14302 and JST CREST Grant Number JPMJCR18J2. The authors gratefully acknowledge the Advanced Characterization Nanotechnology Platform of the University of Tokyo, for the single-crystal X-ray diffraction experiments for **Ph-BBBT-C10**. We also thank Mr. Naoya Toda (AIST) for his technical assistance.

Notes and references

1 J. E. Anthony, *Chem. Rev.*, 2006, **106**, 5028.
2 J. E. Anthony, *Angew. Chemie Int. Ed.*, 2008, **47**, 452.
3 K. Takimiya, S. Shinamura, I. Osaka and E. Miyazaki, *Adv. Mater.*, 2011, **23**, 4347.
4 C. Wang, H. Dong, W. Hu, Y. Liu and D. Zhu, *Chem. Rev.*, 2012, **112**, 2208.
5 K. Takimiya, M. Nakano, M. J. Kang, E. Miyazaki and I. Osaka, *European J. Org. Chem.*, 2013, 217.
6 W. Jiang, Y. Li and Z. Wang, *Chem. Soc. Rev.*, 2013, **42**, 6113.
7 J. Mei, Y. Diao, A. L. Appleton, L. Fang and Z. Bao, *J. Am. Chem. Soc.*, 2013, **135**, 6724.
8 C. Zhang, P. Chen and W. Hu, *Small*, 2016, **12**, 1252.
9 M. Chen, L. Yan, Y. Zhao, I. Murtaza, H. Meng and W. Huang, *J. Mater. Chem. C*, 2018, **6**, 7416.
10 A. Naibi Lakshminarayana, A. Ong and C. Chi, *J. Mater. Chem. C*, 2018, **6**, 3551.
11 H. Dong, X. Fu, J. Liu, Z. Wang and W. Hu, *Adv. Mater.*, 2013, **25**, 6158.
12 S. K. Park, J. H. Kim and S. Y. Park, *Adv. Mater.*, 2018, **30**, 1704759.
13 C. D. Dimitrakopoulos, a. R. Brown and A. Pomp, *J. Appl. Phys.*, 1996, **80**, 2501.
14 H. Klauk, M. Halik, U. Zschieschang, G. Schmid, W. Radlik and W. Weber, *J. Appl. Phys.*, 2002, **92**, 5259.
15 J. Takeya, C. Goldmann, S. Haas, K. P. Pernstich, B. Ketterer and B. Batlogg, *J. Appl. Phys.*, 2003, **94**, 5800.
16 O. D. Jurchescu, M. Popinciuc, B. J. van Wees and T. T. M. Palstra, *Adv. Mater.*, 2007, **19**, 688.
17 V. Podzorov, V. M. Pudalov and M. E. Gershenson, *Appl. Phys. Lett.*, 2003, **82**, 1739.
18 V. Podzorov, S. E. Sysoev, E. Loginova, V. M. Pudalov and M. E. Gershenson, *Appl. Phys. Lett.*, 2003, **83**, 3504.
19 J. Takeya, M. Yamagishi, Y. Tominari, R. Hirahara, Y. Nakazawa, T. Nishikawa, T. Kawase, T. Shimoda and S. Ogawa, *Appl. Phys. Lett.*, 2007, **90**, 102120.
20 K. A. McGarry, W. Xie, C. Sutton, C. Risko, Y. Wu, V. G. Young, J.-L. Brédas, C. D. Frisbie and C. J. Douglas, *Chem. Mater.*, 2013, **25**, 2254.
21 K. Takimiya, H. Ebata, K. Sakamoto, T. Izawa, T. Otsubo and Y. Kunugi, *J. Am. Chem. Soc.*, 2006, **128**, 12604.
22 H. Ebata, T. Izawa, E. Miyazaki, K. Takimiya, M. Ikeda, H. Kuwabara and T. Yui, *J. Am. Chem. Soc.*, 2007, **129**, 15732.
23 G. Schweicher, V. Lemaur, C. Niebel, C. Ruzié, Y. Diao, O. Goto, W.-Y. Lee, Y. Kim, J.-B. Arlin, J. Karpinska, A. R. Kennedy, S. R.

Parkin, Y. Olivier, S. C. B. Mannsfeld, J. Cornil, Y. H. Geerts and Z. Bao, *Adv. Mater.*, 2015, **27**, 3066.
24 G. H. Roche, Y.-T. Tsai, S. Clevers, D. Thuau, F. Castet, Y. H. Geerts, J. J. E. Moreau, G. Wantz and O. J. Dautel, *J. Mater. Chem. C*, 2016, **4**, 6742.
25 C. Yao, X. Chen, Y. He, Y. Guo, I. Murtaza and H. Meng, *RSC Adv.*, 2017, **7**, 5514.
26 T. Yamamoto and K. Takimiya, *J. Am. Chem. Soc.*, 2007, **129**, 2224.
27 M. J. Kang, I. Doi, H. Mori, E. Miyazaki, K. Takimiya, M. Ikeda and H. Kuwabara, *Adv. Mater.*, 2011, **23**, 1222.
28 M. J. Kang, E. Miyazaki, I. Osaka, K. Takimiya and A. Nakao, *ACS Appl. Mater. Interfaces*, 2013, **5**, 2331.
29 M. Sawamoto, M. J. Kang, E. Miyazaki, H. Sugino, I. Osaka and K. Takimiya, *ACS Appl. Mater. Interfaces*, 2016, **8**, 3810.
30 O. D. Jurchescu, D. a. Mourey, S. Subramanian, S. R. Parkin, B. M. Vogel, J. E. Anthony, T. N. Jackson and D. J. Gundlach, *Phys. Rev. B*, 2009, **80**, 085201.
31 Y. Miyata, E. Yoshikawa, T. Minari, K. Tsukagoshi and S. Yamaguchi, *J. Mater. Chem.*, 2012, **22**, 7715.
32 M. Nakano, K. Niimi, E. Miyazaki, I. Osaka and K. Takimiya, *J. Org. Chem.*, 2012, **77**, 8099.
33 T. Okamoto, C. Mitsui, M. Yamagishi, K. Nakahara, J. Soeda, Y. Hirose, K. Miwa, H. Sato, A. Yamano, T. Matsushita, T. Uemura and J. Takeya, *Adv. Mater.*, 2013, **25**, 6392.
34 C. Mitsui, T. Okamoto, H. Matsui, M. Yamagishi, T. Matsushita, J. Soeda, K. Miwa, H. Sato, A. Yamano, T. Uemura and J. Takeya, *Chem. Mater.*, 2013, **25**, 3952.
35 C. Mitsui, T. Okamoto, M. Yamagishi, J. Tsurumi, K. Yoshimoto, K. Nakahara, J. Soeda, Y. Hirose, H. Sato, A. Yamano, T. Uemura and J. Takeya, *Adv. Mater.*, 2014, **26**, 4546.
36 J.-I. Park, J. W. Chung, J.-Y. Kim, J. Lee, J. Y. Jung, B. Koo, B.-L. Lee, S. W. Lee, Y. W. Jin and S. Y. Lee, *J. Am. Chem. Soc.*, 2015, **137**, 12175.
37 Y. Yamaguchi, M. Takubo, K. Ogawa, K.-I. Nakayama, T. Koganezawa and H. Katagiri, *J. Am. Chem. Soc.*, 2016, **138**, 11335.
38 C. Mitsui, H. Tsuyama, R. Shikata, Y. Murata, H. Kuniyasu, M. Yamagishi, H. Ishii, A. Yamamoto, Y. Hirose, M. Yano, T. Takehara, T. Suzuki, H. Sato, A. Yamano, E. Fukuzaki, T. Watanabe, Y. Usami, J. Takeya and T. Okamoto, *J. Mater. Chem. C*, 2017, **5**, 1903.
39 H.-Y. Chen, G. Schweicher, M. Planells, S. M. Ryno, K. Broch, A. J. P. White, D. Simatos, M. Little, C. Jellett, S. J. Cryer, A. Marks, M. Hurhangee, J.-L. Brédas, H. Sirringhaus and I. McCulloch, *Chem. Mater.*, 2018, **30**, 7587.
40 G. R. Desiraju and A. Gavezzotti, *J. Chem. Soc. Chem. Commun.*, 1989, 621.
41 G. R. Desiraju and A. Gavezzotti, *Acta Crystallogr. Sect. B Struct. Sci.*, 1989, **45**, 473.
42 M. Mas-Torrent and C. Rovira, *Chem. Rev.*, 2011, **111**, 4833.
43 W. Jiang, Y. Li and Z. Wang, *Chem. Soc. Rev.*, 2013, **42**, 6113.
44 J. Yang, S. De, J. E. Campbell, S. Li, M. Ceriotti and G. M. Day, *Chem. Mater.*, 2018, **30**, 4361.
45 J. Yang, N. Li and S. Li, *CrystEngComm*, 2019, **21**, 6173.
46 F. Musil, S. De, J. Yang, J. E. Campbell, G. M. Day and M. Ceriotti, *Chem. Sci.*, 2018, **9**, 1289.
47 M. Klues and G. Witte, *CrystEngComm*, 2018, **20**, 63.
48 J. E. Anthony, J. S. Brooks, D. L. Eaton and S. R. Parkin, *J. Am. Chem. Soc.*, 2001, **123**, 9482.
49 J. E. Anthony, D. L. Eaton and S. R. Parkin, *Org. Lett.*, 2002, **4**, 15.
50 M. M. Payne, S. R. Parkin, J. E. Anthony, C.-C. Kuo and T. N. Jackson, *J. Am. Chem. Soc.*, 2005, **127**, 4986.
51 M. J. Kang, T. Yamamoto, S. Shinamura, E. Miyazaki and K. Takimiya, *Chem. Sci.*, 2010, **1**, 179.
52 M. S. Kazantsev, A. A. Beloborodova, E. S. Frantseva, T. V. Rybalova, V. G. Konstantinov, I. K. Shundrina, D. Y. Paraschuk and E. A. Mostovich, *CrystEngComm*, 2017, **19**, 1809.
53 C. Kitamura, T. Ohara, N. Kawatsuki, A. Yoneda, T. Kobayashi, H. Naito, T. Komatsu and T. Kitamura, *CrystEngComm*, 2007, **9**, 644.
54 M. Kanno, Y. Bando, T. Shirahata, J. Inoue, H. Wada and T. Mori, *J. Mater. Chem.*, 2009, **19**, 6548.
55 J. Nagakubo, M. Ashizawa, T. Kawamoto, A. Tanioka and T. Mori, *Phys. Chem. Chem. Phys.*, 2011, **13**, 14370.
56 T. Higashino, Y. Akiyama, H. Kojima, T. Kawamoto and T. Mori, *Crystals*, 2012, **2**, 1222.
57 H. Mori, X.-C. Chen, N.-H. Chang, S. Hamao, Y. Kubozono, K. Nakajima and Y. Nishihara, *J. Org. Chem.*, 2014, **79**, 4973.
58 T. Higashino, M. Dogishi, T. Kadoya, R. Sato, T. Kawamoto and T. Mori, *J. Mater. Chem. C*, 2016, **4**, 5981.
59 T. Higashino, A. Ueda and H. Mori, *New J. Chem.*, 2019, **43**, 884.
60 V. S. Vyas, R. Gutzler, J. Nuss, K. Kern and B. V. Lotsch, *CrystEngComm*, 2014, **16**, 7389.
61 P. V. Hatcher, J. H. Reibenspies, R. C. Haddon, D. Li, N. Lopez and X. Chi, *CrystEngComm*, 2015, **17**, 4172.
62 T. Kadoya, S. Mano, A. Hori, K. Tahara, K. Sugimoto, K. Kubo, M. Abe, H. Tajima and J. Yamada, *Org. Electron.*, 2020, **78**, 105570.
63 H. Inokuchi, G. Saito, P. Wu, K. Seki, T. B. Tang, T. Mori, K. Imaeda, T. Enoki, Y. Higuchi, K. Inaka and N. Yasuoka, *Chem. Lett.*, 1986, **15**, 1263.
64 F. Garnier, A. Yassar, R. Hajlaoui, G. Horowitz, F. Deloffre, B. Servet, S. Ries and P. Alnot, *J. Am. Chem. Soc.*, 1993, **115**, 8716.
65 T. E. Clark, M. Makha, J. J. McKinnon, A. N. Sobolev, M. A. Spackman and C. L. Raston, *CrystEngComm*, 2007, **9**, 566.
66 T. Izawa, E. Miyazaki and K. Takimiya, *Adv. Mater.*, 2008, **20**, 3388.
67 S. Inoue, H. Minemawari, J. Tsutsumi, M. Chikamatsu, T. Yamada, S. Horiuchi, M. Tanaka, R. Kumai, M. Yoneya and T. Hasegawa, *Chem. Mater.*, 2015, **27**, 3809.
68 H. Minemawari, M. Tanaka, S. Tsuzuki, S. Inoue, T. Yamada, R. Kumai, Y. Shimoi and T. Hasegawa, *Chem. Mater.*, 2017, **29**, 1245.
69 S. Inoue, S. Shinamura, Y. Sadamitsu, S. Arai, S. Horiuchi, M. Yoneya, K. Takimiya and T. Hasegawa, *Chem. Mater.*, 2018, **30**, 5050.
70 T. Higashino, S. Inoue, Y. Sadamitsu, S. Arai, S. Horiuchi and T. Hasegawa, *Chem. Lett.*, 2019, **48**, 453.
71 H. Iino, T. Usui and J.-I. Hanna, *Nat. Commun.*, 2015, **6**, 6828.
72 Y. He, M. Sezen, D. Zhang, A. Li, L. Yan, H. Yu, C. He, O. Goto, Y.-L. Loo and H. Meng, *Adv. Electron. Mater.*, 2016, **2**, 1600179.
73 K. He, W. Li, H. Tian, J. Zhang, D. Yan, Y. Geng and F. Wang, *ACS Appl. Mater. Interfaces*, 2017, **9**, 35427.
74 S. Arai, S. Inoue, T. Hamai, R. Kumai and T. Hasegawa, *Adv. Mater.*, 2018, **30**, 1707256.
75 S. Guo, Y. He, I. Murtaza, J. Tan, J. Pan, Y. Guo, Y. Zhu, Y. He and H. Meng, *Org. Electron.*, 2018, **56**, 68.
76 S. Arai, K. Morita, J. Tsutsumi, S. Inoue, M. Tanaka and T. Hasegawa, Adv. Funct. Mater., 2020, 30, 1906406.
77 S. Tsuzuki, K. Honda, T. Uchimaru, M. Mikami and K. Tanabe, *J. Am. Chem. Soc.*, 2002, **124**, 104.
78 S. Tsuzuki, K. Honda, T. Uchimaru and M. Mikami, *J. Chem. Phys.*, 2006, **124**, 114304.
79 H. Ebata, E. Miyazaki, T. Yamamoto and K. Takimiya, *Org. Lett.*, 2007, **9**, 4499.
80 P. Gao, D. Beckmann, H. N. Tsao, X. Feng, V. Enkelmann, W. Pisula and K. Müllen, *Chem. Commun.*, 2008, 1548.
81 M. Maroncelli, S. P. Qi, H. L. Strauss and R. G. Snyder, *J. Am. Chem. Soc.*, 1982, **104**, 6237.
82 L. Loots and L. J. Barbour, *CrystEngComm*, 2012, **14**, 300.

83 M. D. Curtis, J. Cao and J. W. Kampf, *J. Am. Chem. Soc.*, 2004, **126**, 4318.
84 E.-G. Kim, V. Coropceanu, N. E. Gruhn, R. S. Sánchez-Carrera, R. Snoeberger, A. J. Matzger and J.-L. Brédas, *J. Am. Chem. Soc.*, 2007, **129**, 13072.
85 X. Zhang, X. Yang, H. Geng, G. Nan, X. Sun, J. Xi and X. Xu, *J. Comput. Chem.*, 2015, **36**, 891.
86 S. Canola and F. Negri, *J. Phys. Chem. C*, 2015, **119**, 11499.
87 Y. Zang, D. Huang, C. Di and D. Zhu, *Adv. Mater.*, 2016, **28**, 4549.
88 S.-F. Yang, X. Zhang, P.-L. Chen, Z.-T. Liu, J.-W. Tian, G.-X. Zhang and D.-Q. Zhang, *Adv. Electron. Mater.*, 2017, **3**, 1700120.
89 B. Peng, S. Huang, Z. Zhou and P. K. L. Chan, *Adv. Funct. Mater.*, 2017, **27**, 1700999.
90 T. Hamai, S. Arai, H. Minemawari, S. Inoue, R. Kumai and T. Hasegawa, *Phys. Rev. Appl.*, 2017, **8**, 054011.
91 CrysAlisPro Software System; Rigaku Oxford Diffraction; Rigaku Corporation: Oxford, UK, 2016.
92 M. C. Burla, R. Caliandro, M. Camalli, B. Carrozzini, G. L. Cascarano, L. De Caro, C. Giacovazzo, G. Polidori and R. Spagna, *J. Appl. Crystallogr.*, 2005, **38**, 381.
93 G. M. Sheldrick, *Acta Crystallogr. Sect. A Found. Crystallogr.*, 2008, **64**, 112.
94 F. L. Hirshfeld, *Theor. Chim. Acta*, 1977, **44**, 129.
95 J. J. McKinnon, D. Jayatilaka and M. A. Spackman, *Chem. Commun.*, 2007, 3814.
96 M. A. Spackman and J. J. McKinnon, *CrystEngComm*, 2002, **4**, 378.
97 M. J. Turner, J. J. McKinnon, S. K. Wolff, D. J. Grimwood, P. R. Spackman, D. Jayatilaka, M. A. Spackman, *CrystalExplorer17*, University of Western Australia, 2017, http://crystalexplorer.scb.uwa.edu.au/.
98 M. J. Frisch, *et al.*, Gaussian 16: Wallingford, CT, 2016.
99 S. Grimme, J. Antony, S. Ehrlich and H. Krieg, *J. Chem. Phys.*, 2010, **132**, 154104.
100 B. J. Ransil, *J. Chem. Phys.*, 1961, **34**, 2109.
101 S. F. Boys and F. Bernardi, *Mol. Phys.*, 1970, **19**, 553.
102 ADF: powerful DFT code for modeling molecules; Scientific Computing and Modeling: Amsterdam; https://www.scm.com.

The table of contents entry

Title

Architecting layered molecular packing in substituted benzobisbenzothiophene (BBBT) semiconductor crystals

Authors

Toshiki Higashino, Shunto Arai, Seiji Tsuzuki, Yukihiro Shimoi, Sachio Horiuchi, Tatsuo Hasegawa, and Reiko Azumi

ToC figure (graphic maximum size 8 cm x 4 cm and one sentence of text, maximum 20 words, highlighting the novelty of the work)

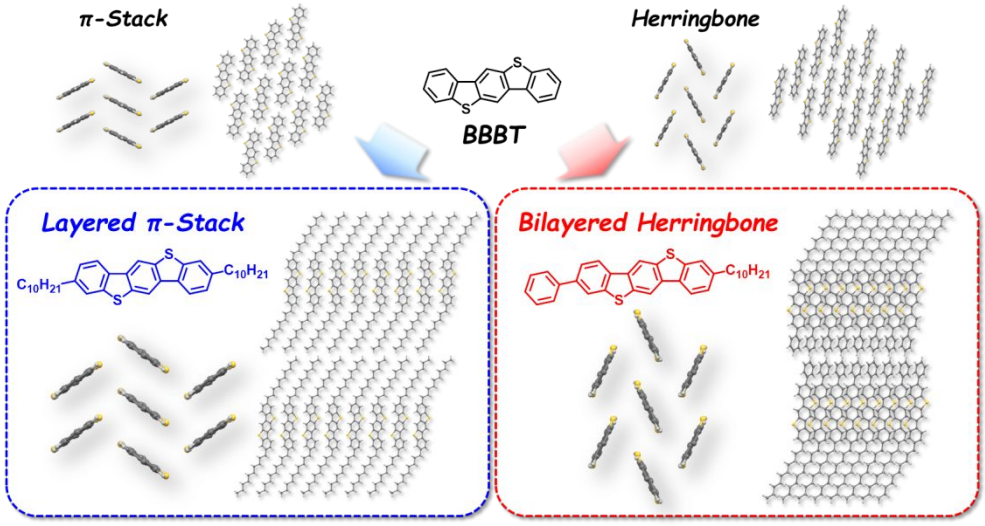

80 x 40 mm

To assist the editor assessing your manuscript, please provide 1-2 sentences stating how your work furthers understanding of the design and behaviour of crystalline materials

Construction of layered molecular packing structures in benzobisbenzothiophene (BBBT), which itself does not show layered crystallinity, was achieved by employing long-alkyl and phenyl substitutions, leading to high-performance organic thin-film transistors.